INORGANIC CHEMISTRY FRONTIERS

RESEARCH ARTICLE

View Article Online
View Journal | View Issue

Cite this: *Inorg. Chem. Front.*, 2022, **9**, 4413

Polyoxometalates with tunable third-order nonlinear optical and superbroadband optical limiting properties†‡

Long-Sheng Wang, *[a,b,e] Yue Wang,[a,b] Chun-Lin Lv,[c] Chao Guo,[a] Fang-Yuan Xing,[b] Yu-Jia Dong,[a] Zheng Xie, *[b] Shu-Yun Zhou[b] and Yong-Ge Wei *[d]

In order to tune the intrinsic third-order nonlinear optical (NLO) properties of polyoxometalates (POMs), we adopted a strategy of substituting addenda atoms of POMs to obtain a class of polyoxomolybdovanadates, $[TBA]_3[VMo_5O_{19}]$ (**V_1Mo_5**), $[TBA]_4[V_8Mo_2O_{28}]\cdot 2CH_3CN$ (**V_8Mo_2**) and $[TBA]_4[HV_9MoO_{28}]\cdot 2CH_3CN$ (**V_9Mo_1**) (TBA = tetrabutylammonium). Their structures were determined by single crystal X-ray diffraction and further characterized by FT-IR, Raman, UV-vis, diffuse reflection, HR MS, XPS, ICP-MS, CHN analysis and so on. The *Z*-scan curves of all compounds in a suspension of propanetriol demonstrate typical nonlinear absorption (NLA) irradiated by a laser at 532 nm and 1064 nm, which can be tuned by the substitution of addenda atoms in POMs. Among those, **V_9Mo_1** possesses the smallest transmittance and largest nonlinear absorption coefficient. **V_9Mo_1**-doped organically modified silica (ORMOSIL) gel glasses have NLA and optical limiting (OL) properties that could be tuned by changing the doping concentration of **V_9Mo_1**. In particular, **V_9Mo_1** exhibits an unusual superbroadband OL performance in the visible and long-wavelength near-infrared regions (532–2150 nm). To the best of our knowledge, this is the first example of a superbroadband optical limiter based on crystalline metal cluster compounds. Our current work not only provides a series of polyoxomolybdovanadates and **V_9Mo_1**-doped gel glasses with tunable third-order NLO properties and superbroadband OL performance but also affords a feasible strategy to tune the third-order NLO properties of POMs *via* the substitution of addenda atoms.

Received 26th April 2022,
Accepted 23rd June 2022

DOI: 10.1039/d2qi00899h

rsc.li/frontiers-inorganic

Introduction

With the rapid development of laser techniques and the coming of the photon era, third-order nonlinear optical (NLO) materials have drawn increasing research attention because of their widespread application in optical devices with optical limiting (OL) and shaping features, optical switches, electro-optical signal processing, optical information processing and so on.[1,2] Up to now, many non-crystalline materials including semiconductors, carbon-based materials, black phosphorus, conjugated organic molecules or polymers, metal oxides and so on[1] have been reported to exhibit different third-order NLO properties, such as saturable absorption (SA), reverse saturable absorption (RSA),[3] optical Kerr effect,[4] nonlinear scattering (NLS), and nonlinear refraction (NLR).[5] Recently, Zhang *et al.* reported that 2D graphdiyne,[6] few-layer tin sulphide,[7] and few-layer bismuthene,[8] which exhibit giant Kerr nonlinearity, can be used as passive photonic diodes in all optical switching and wavelength conversion. Among those materials, only a few (mainly carbon-based, two dimensional,[9] especially graphene) exhibit a broadband optical limiting response. The broadband optical limiters are of importance for laser protection because they can protect the eyes or costly instruments from damage due to a laser in a wide range of wavelengths. Hitherto, graphene has been undoubtedly the best broadband optical limiter due to its excellent broadband optical limiting performance[10] and lowest OL threshold. However, the self-aggre-

[a]*School of Material and Chemical Engineering, Hubei Provincial Key Laboratory of Green Materials for Light Industry, Hubei University of Technology, Wuhan, 430068 Hubei Province, P.R. China. E-mail: wls@mail.tsinghua.edu.cn*
[b]*Key Laboratory of Photochemical Conversion and Optoelectronic Materials, Technical Institute of Physics and Chemistry, Chinese Academy of Sciences, Beijing, 100190, China. E-mail: zhengxie@mail.ipc.ac.cn*
[c]*Department of Chemistry, School of Life and Environmental Sciences, Minzu University of China, Beijing, 100081, China*
[d]*Key Lab of Organic Optoelectronics & Molecular Engineering of Ministry of Education, Department of Chemistry, School of Science, Tsinghua University, Beijing, 100084, China. E-mail: yonggewei@mail.tsinghua.edu.cn*
[e]*State Key Laboratory of Structural Chemistry, Fujian Institute of Research on the Structure of Matter, Chinese Academy of Sciences, Fuzhou, 350002 Fujian Province, China*

† Dedicated to the 70th anniversary of the Hubei University of Technology.

‡ Electronic supplementary information (ESI) available. CCDC 2080750–2080752. For ESI and crystallographic data in CIF or other electronic format see DOI: https://doi.org/10.1039/d2qi00899h

gation property of graphene requires modification by suitable functional groups for better dispersion in solution or solid matrices.[11] Moreover, the strong light absorption ability of carbon materials not only restricts their doping level in solid matrices[12] but also lowers the transparence of the corresponding devices. Therefore, it is still very significant to develop non-carbon materials with broadband OL.

To date, only a small amount of effort has been devoted to third-order NLO crystalline compounds like molecular clusters.[13,14] Heterometallic clusters of Mo/W/Cu/S[15] with cubane-like,[16] nest, twin-nest and planar open shape, have been found to demonstrate excellent NLO response with a large third-order NLO susceptibility and low laser limiting threshold to a nanosecond laser at 532 nm.[17] Recently, a series of Al_{32}-oxo clusters with hydrotalcite-like structure has been reported to exhibit NLA and OL to a nanosecond laser at 532 nm.[18] To the best of our knowledge, no molecular clusters with broadband OL have been reported up to now.

Polyoxometalates (POMs) are a large class of isolated metal–oxygen clusters consisting of early-transition metal (V, Mo, W, Nb, Ta) ions in their highest oxidation state (+5 or +6) and oxo ligands.[19,20] POMs have tremendous structural diversity (the metal nuclearities ranging from 6 to 368), large cluster-size span (ranging from 0.8 nm to 6.0 nm)[21] and unmatched composition variability (many transition metal ions and non-metal cations can be incorporated in polyoxometalates).[22] POMs demonstrate interesting super acidity, biological activity, and magnetic, chiral, reversible redox, electronic and photoactive properties depending on their various structures and compositions. Therefore, POMs have been drawing increasing research attention due to their attractive potential applications in catalysis,[23–25] chirality,[26–28] water oxidation,[29] POM-MOF,[30–32] self-assembly[33] and self-recognition,[34] and so on. Moreover, many POMs with large delocalized π electrons are potential NLO materials[35–37] in terms of the consensus that delocalized π-conjugated systems possess a strong NLO response. However, only a very small amount of effort has been made to investigate their NLO properties.[38,39] Recently, two strategies have been developed to prepare POM-based third-order NLO materials. The first one is to introduce organic components with excellent NLO properties (*i.e.* porphyrin,[40] phthalocyanine,[41] or tetrathiafulvalene) *via* a noncovalent bond[42,43] or a covalent bond,[44–46] which can efficiently enhance third-order NLO properties of the hybrids by the introduction of such organic components. The second one is to construct POM-based coordination polymers using POMs as anion templates or linkers.[47,48] Nonetheless, it is still a great challenge to improve the intrinsic NLO properties of POMs without the assistance of organic components possessing excellent third-order NLO properties.

On the other hand, NLO properties can be well studied in solution, but it is essential to incorporate NLO materials into a solid-state matrix for further practical application.[1,49] One attractive approach is the sol–gel glasses technique, especially, organically modified silica (ORMOSIL) gel glasses.[50] It is an ideal matrix for a solid device due to its advantages including a high threshold of laser damage, good transparency in the UV-LW NIR region, and excellent optical, thermal and mechanical properties.[51,52] Moreover, such hybrid glass materials have multiple solid forms (coatings, films, nanoparticles, fibers, and aerogel monoliths) and the gel itself can also be coated on different substrates such as ceramics, metals and common glasses.[51,52] However, no POMs have been introduced into gel glasses up to now.

Inspired by the fact that the doping of some materials by hetero atoms (*i.e.* VO_2 doped by a hetero metal atom,[53] graphene doped by B or N atoms[54,55]) can improve their nonlinear optical properties, we choose two classic POMs, hexamolybdate (**Mo_6**) and decavanadate (**V_{10}**) (Scheme 1), with delocalized π electrons as a platform for POMs to prepare their addenda metal atom substituted POMs (**Mo_6** by vanadium, **V_{10}** by molybdenum), namely, polyoxomolybdovanadates, and further investigate their NLO properties. Three polyoxomolybdovanadates, $[TBA]_3[VMo_5O_{19}]$ (**V_1Mo_5**), $[TBA]_4[Mo_2V_8O_{28}]$ (**V_8Mo_2**), and $[TBA]_4[HV_9MoO_{28}]$ (**V_9Mo_1**) (TBA = tetrabutylammonium), have been prepared through a general procedure of acidification–precipitation–crystallization in modest to high yields. They have been characterized by single crystal X-ray diffraction, HR MS, FT-IR, Raman, UV-vis, XPS, ICP-MS and CHN analysis. Interestingly, these polyoxomolybdovanadates exhibit modulated third-order NLO properties through controlling the substitution of addenda atoms. Moreover, we prepared the **V_9Mo_1**-doped gel glasses with different concentrations and measured their NLO properties and optical limiting (OL) behaviors. In this paper, we report the preparation, structures, characterization, NLO properties and OL behaviors of $[TBA]_3[VMo_5O_{19}]$ (**V_1Mo_5**), $[TBA]_4[Mo_2V_8O_{28}]$ (**V_8Mo_2**), $[TBA]_4[HV_9MoO_{28}]$ (**V_9Mo_1**) and **V_9Mo_1**-doped gel glasses.

Experimental

General

All chemicals and reagents were of analytical grade and obtained commercially from Aladdin Reagent Co., Ltd, Ji'nan Henghua Reagent Co., Ltd or Sinopharm Chemical Reagent Co., Ltd, which were used as received without further purifications except as otherwise noted. Fourier transform infrared (FT-IR) spectra were obtained on an Excalibur HE 3100

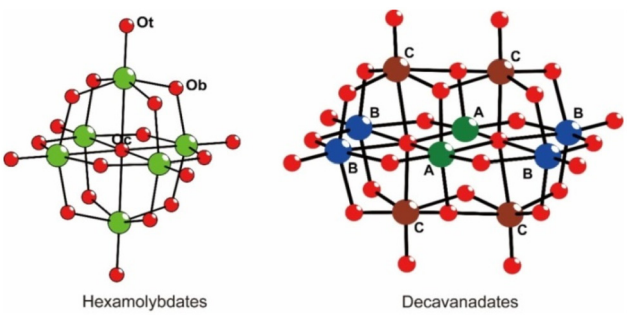

Scheme 1 Ball-stick diagrams of hexamolybdates and decavanadates.

(Varian) using a pressed KBr pellet in the wavenumber range of 400–4000 cm^{-1}. Raman spectra were measured on an XpolRA PLUS confocal Raman microscope (Horiba) by adhering these finely ground sample powders on double faced adhesive tape in the wavenumber range of 400–4000 cm^{-1}. UV-Vis absorption spectra and transmission spectra were obtained on a Varian Cary 5000 UV-visible-near infrared absorption spectrophotometer. Diffuse reflection spectra were obtained on a UV-7000 spectrometer in the wavenumber range of 200–2500 cm^{-1}. Gas chromatography high resolution mass spectra (HR MS) were obtained with a Thermo Scientific Q ExactiveTM GC Orbitrap system using their acetonitrile solutions. X-ray photoelectron spectroscopy (XPS) was performed on an ESCALAB 250Xi (Thermo Scientific, UK) using monochromatic Al Kα as the excitation source. A pass energy of 25 eV was used in the XPS measurement. The base pressure of the analysis chamber was less than 6.7×10^{-8} Pa. All spectra were calibrated using the binding energy of C 1s (285.0 eV) as a reference. Inductively coupled plasma emission spectroscopy (ICP MS) was performed using a Varian 710-OES (USA). Scanning electron microscope (SEM) images were obtained on a Hitachi SU8010 scanning electron microscope. Transmission electron microscope (TEM) images were obtained on a Thermo Scientific Talos F200X transmission electron microscope. Measurements of their third-order nonlinear optical properties were obtained on a Lab170 Nd:YAG (Spectra-Physics, USA) pulsed laser system employed as the light source with a wavelength of 532 and 1064 nm (beam size: 5–6 mm), pulse duration of 10 ns and repetition rate of 10 Hz. The waist radius of 532 and 1064 nm was 13.5 μm and 27 μm, respectively. Optical limiting tests of the gel glasses were carried out using two laser systems: the Lab170 Nd:YAG pulsed laser was used to measure the nonlinear optical properties at 532 and 1064 nm and the PremiScan/240/MB-ULD (Spectra-Physics, USA) optical parametric oscillator was used to measure the optical limiting properties at 2150 nm.

These samples were dispersed beforehand in glycerol to form a suspension, which was placed in a quartz cuvette with a thickness of 1 mm and fixed to a stepper motor controlled by a computer. The quartz cuvette was moved along the *Z* axis based on the focus. In the closed-aperture measurement, the self-limiting effect is demonstrated by the beam translation to achieve self-focusing or self-defocusing. When the sample is moved from $-Z$ to $+Z$, the normalized transmittance peaks and valleys appear in turn, indicating self-focusing whereas self-defocusing is observed *vice versa*. Further, the OL tests are carried out with an open aperture *Z*-scan equipment. The solid glass devices doped with different percentages are fixed on the stepper motor, and the stepper motor is moved to the laser focus.

General synthetic procedure

Stoichiometric Na_3VO_4 and $NaMoO_4{\cdot}2H_2O$ were dissolved in 20.0 mL of deionized water to form a colorless solution, which was acidified using HCl (3 mol L^{-1}) to form a yellow solution. To this yellow solution, a solution of TBA in 7.0 ml of deionized water was added slowly. Lots of yellow precipitation appeared rapidly, which was stirred for another 2 hours and filtered to yield lots of yellow solids. The obtained yellow solids were successively washed with water, ethanol, and diethyl ether, and dried for 12 hours in a vacuum drying oven. The crude products were dissolved in 10 mL of acetonitrile and diffused by diethyl ether.

$(TBA)_3[VMo_5O_{19}]$ (VMo_5). 1.25 g of Na_3VO_4 (6.8 mmol), 8.23 g of $NaMoO_4{\cdot}2H_2O$ (34.0 mmol), and 7.0 g of TBA (21.0 mmol) are used to prepare VMo_5. Light yellow block crystals were obtained that were collected by filtration and washed with diethyl ether. 4.13 g, 39%. CHN analysis found (%): C, 37.20; H, 6.99; N, 2.67; calc. for $C_{48}H_{108}N_3O_{19}Mo_5V$: C, 36.91; H, 6.97; N, 2.69%. UV-Vis $\lambda_{max}(CH_3CN)$: 231 (ε/dm^3 mol^{-1} cm^{-1}, 47 500), 264 (32 500), 331 (14 400). FT-IR (KBr pellet, cm^{-1}): 2960 (vs), 2874 (s), 1636 (vs), 1482 (vs), 1384 (m), 1152 (s), 977 (w), 935 (s, sh), 887 (w), 793 (vs), 736 (m), 572 (w). Raman (irradiated by 532 nm laser, cm^{-1}): 2928, 2876, 1462, 1318, 1135, 1055, 974, 939, 806, 595. HR MS *m*/*z*: $[M + H]^+$ calcd for $C_{48}H_{109}Mo_5N_3O_{19}V$, 1563.2467, found 1563.2407; $[M + TBA]^+$ calcd for $C_{64}H_{144}Mo_5N_4O_{19}V$, 1804.5164, found 1804.5240.

$(TBA)_4[V_8Mo_2O_{28}]{\cdot}2CH_3CN$ (V_8Mo_2). 3.75 g of Na_3VO_4 (20.4 mmol), 2.11 g of $NaMoO_4{\cdot}2H_2O$ (8.7 mmol), and 6.0 g of TBA (18.7 mmol) are used to prepare V_8Mo_2. Light yellow block crystals appeared on the wall of the test tube, which were filtered and washed with diethyl ether. 5.08 g, 96%. CHN analysis found: C, 38.02; H, 7.08; N, 2.88; calc. for $C_{64}H_{144}Mo_2N_4O_{28}V_8$: C, 38.10; H, 7.19; N, 2.78%. UV-Vis $\lambda_{max}(CH_3CN)$: 231 nm (ε/dm^3 mol^{-1} cm^{-1}, 54 900), 352 (12 100). FT-IR (KBr pellet, cm^{-1}): 2961 (vs), 2872 (s), 1636 (m), 1481 (vs), 1384 (s), 1151 (s), 1029 (w), 982 (w), 966 (s, sh), 938 (m), 842 (s), 757 (m), (m). Raman (irradiated by 532 nm laser, cm^{-1}): 2967, 2928, 2879, 1454, 1326, 1112, 1059, 986, 831, 775, 724, 596, 441. HR MS *m*/*z*: $[M + 2TBA]^{2+}$ calcd for $C_{96}H_{216}Mo_2N_6O_{28}V_8$, 1250.9656, found 1250.9719; $[M + H]^+$ calcd for $C_{64}H_{145}Mo_2N_4O_{28}V_8$, 2018.3765, found 2018.3716; $[M + TBA]^+$ calcd for $C_{80}H_{180}Mo_2N_5O_{28}V_8$, 2261.6596, found 2261.6541.

$(TBA)_4[HV_9MoO_{28}]{\cdot}2CH_3CN$ (V_9Mo_1). 3.75 g of Na_3VO_4 (20.4 mmol), 0.55 g of $NaMoO_4{\cdot}2H_2O$ (2.3mmol), and 6.0 g of TBA (18.7 mmol) are used to prepare V_9Mo_1. Light yellow block crystals were formed, which were filtered and washed with diethyl ether. 2.04 g, 40.5%. CHN analysis found: C, 38.87; H, 7.50; N; calc. 2.80 for $C_{64}H_{145}MoN_4O_{28}V_9$: C, 38.95; H, 7.41; N, 2.84%. UV-Vis $\lambda_{max}(CH_3CN)$: 230 (ε/dm^3 mol^{-1} cm^{-1}, 57 600), 347 (13 300). FT-IR (KBr pellet, cm^{-1}): 2961 (s), 2933 (w), 2872 (m), 1638 (w), 1618 (w), 1481 (s), 1384 (m), 1151 (w), 1108 (w), 982 (w), 966 (vs, sh), 939 (m), 843 (s), 757(m), 587(m). Raman (irradiated by 532 nm laser, cm^{-1}): 2931, 2882, 1458, 1318, 1131, 993, 824, 727, 591, 531. HR MS *m*/*z*: $[M + 2TBA]^{2+}$ calcd for $C_{96}H_{216}MoN_6O_{28}V_9$, 1229.1961, found 1229.4815; $[M + H]^+$ calcd. for $C_{64}H_{146}MoN_4O_{28}V_9$, 1975.4231, found 1975.4501; $[M + TBA]^+$ calcd. for $C_{80}H_{181}MoN_5O_{28}V_9$, 2216.7005, found 2216.6776.

Preparation of ORMOSIL gel glass

V_9Mo_1-doped ORMOSIL gel glasses were prepared by adding the fine-ground samples into the gel that had been pre-pre-

pared by the hydrolysis and polycondensation reaction of methyltriethoxysilane (MTES) in an acidic solution (H_2O, acetic acid, pH = 2.5) according to a published procedure.[51] The mixture of MTES/ethanol/water in the molecular ratio of 1 : 3 : 3 was stirred overnight until half of the solvent was left after evaporation, and the mixture was stirred for another 3 days to obtain a silica gel. Then, **V_9Mo_1** was added into the silica gel in different concentrations to prepare 0.01%–1% **V_9Mo_1**-doped gel glasses. Finally, the gel was transferred to a polypropylene cell and dried at room temperature for 4 weeks, and the final **V_9Mo_1**-doped gel glasses were obtained. The blank ORMOSIL gel glass was prepared by a similar procedure without the addition of **V_9Mo_1**.

Single crystal X-ray diffraction

Suitable crystals were covered with an inert oil, mounted on glass fibers and transferred onto the diffractometer rapidly. All X-ray diffraction data were collected on a Bruker SMART APEX CCD diffractometer using graphite-monochromatized Mo Kα radiation (λ = 0.71073 Å) at a low temperature (150 ± 2 K). Data collection and data reduction, cell refinement and experiential absorption correction for all compounds were performed using the software packages SMART and SAINT. Structures of all compounds were solved by direct methods or heavy atom methods and refined against F^2 by full matrix least squares. All non-hydrogen atoms, except some disordered atoms, were refined anisotropically. The occupancy ratios of vanadium and molybdenum were refined using a free variable with a restrained occupancy sum (Mo occupancy ratio was restrained to 2.5 for **V_1Mo_5**, 0.5 for **V_8Mo_2**, and 1.0 for **V_9Mo_1**), and sites with very low occupancies or negative occupancies of molybdenum are defined as fully occupied by a vanadium atom, or else they were confirmed as position-disordered sites. Hydrogen atoms of all carbon atoms were generated geometrically. All calculations were performed using the SHELXS-97 and SHELXL-97 program packages.[56–58]

Results and discussion

Syntheses of polyoxomolybdovanadates

Although some simple polyoxomolybdovanadates (*i.e.* $[VMo_5O_{19}]^{3-}$, $[V_2Mo_4O_{19}]^{5-}$, $[V_9MoO_{28}]^{5-}$, $[V_8Mo_2O_{28}]^{4-}$ and so on) had been observed in the aqueous solution of stoichiometric vanadates/molybdates by NMR spectroscopy and potentiometry,[59,60] their preparation and isolation are still faced with significant difficulty due to the coexistence of multiple polyanions in their aqueous solutions. To date, only a few polyoxomolybdovanadates, such as $K_7[V_5Mo_8O_{40}]\cdot 8H_2O$,[61] $Na_6[V_2Mo_6O_{26}]\cdot 16H_2O$,[62] and $K_6[V_8Mo_4O_{36}]\cdot 12H_2O$,[63] have been isolated as crystals. The direct reaction of metal oxide (MoO_3 or V_2O_5) with molybdates or vanadates in a non-aqueous solvent can yield some polyoxomolybdovanadates in a low yield. For example, $[TBA]_3[VMo_5O_{19}]$ was prepared by the refluxing of $[N(C_4H_9)_4]_4[Mo_8O_{26}]$, V_2O_5 and the methanol solution of $[(n\text{-}C_4H_9)_4N]\cdot OH$ in acetonitrile with a yield of *ca.* 22%.[64] $[(CH_3)_4N]_4[H_2MoV_9O_{28}]Cl\cdot 6H_2O$ was obtained through the reaction of MoO_3 and NH_4VO_4 in a yield of *ca.* 0.83%.[65] Recently, Ritchie *et al.* developed a microwave-assisted method to afford $(TBA)_3[V_7Mo_3O_{28}]$ and $(TBA)_2[V_3Mo_3O_{16}(C_5H_9O_3)]$ in a non-aqueous solvent.[66] Therefore, it is still very valuable to develop a convenient and common method to prepare polyoxomolybdovanadates for further applications.

Herein, we developed a convenient method towards polyoxomolybdovanadates ($[TBA]_3[VMo_5O_{19}]$ (**VMo_5**), $[TBA]_4[Mo_2V_8O_{28}]$ (**V_8Mo_2**), and $[TBA]_4[HV_9MoO_{28}]$ (**V_9Mo_1**)) with modest to high yields. They were obtained by a general procedure of acidification–precipitation–crystallization, namely, acidification of stoichiometric Na_3VO_4 and Na_2MoO_4 in an aqueous solution by HCl, precipitation by a quaternary ammonium salt of TBA, then crystallization through the diffusion of Et_2O into their acetonitrile solution. **VMo_5** and **V_9Mo_1** can be obtained as block crystals (yellow for **VMo_5** and orange for **V_9Mo_1**) in a high yield through the corresponding stoichiometric reaction of Na_3VO_4/Na_2MoO_4 (1 : 5 for **VMo_5**, 9 : 1 for **V_9Mo_1**). Interestingly, the reaction of Na_3VO_4/Na_2MoO_4 in the ratio of 7 : 3 affords **V_8Mo_2** rather than $[TBA]_3[V_7Mo_3O_{28}]$ (**V_7Mo_3**).

Crystal structure

Single crystal X-ray diffraction (XRD) structural analysis reveals that **VMo_5** with the molecular formula $(TBA)_3[VMo_5O_{19}]$ possesses an anion cluster similar to Lindqvist POMs. It crystallizes in the monoclinic system, *C*2/*c* space group. There are two half anion clusters of $[VMo_5O_{19}]^{3-}$ and three TBA cations in their asymmetric unit. As shown in Fig. 1(a and b), the anion clusters possess the typical Lindqvist structure with a symmetric center on the central oxo ligand. It can be viewed as one molybdenum atom in the hexamolybdate substituted by one vanadium atom. However, the position of the vanadium in the anion cluster is not determinate owing to the crystallographically imposed symmetry of O_h. The refined occupancy of molybdenum atoms shows that the occupancy of Mo1, Mo2, Mo3, Mo4, Mo5 and Mo6 in **VMo_5** is 0.88003, 0.87851, 0.74087, 0.86230, 0.82888 and 0.80860, respectively. The occupation ratios of molybdenum atoms are close to the random distribution (0.8333 for **VMo_5**) in those positions, indicating that the distribution of molybdenum atoms in these positions is random. All metal atoms are six-coordinated with one terminal oxygen atom (O_t), four bridged oxygen atoms (O_b) and one central oxygen atom (O_c) to form a distorted octahedron. The bond lengths of M–O_t (1.664(3)–1.683(3) Å), M–O_b (1.875(2)–1.957(3) Å) and M–O_c (2.296(2)–2.3088(5) Å), and the separation between adjacent metal atoms in **VMo_5** are slightly shorter than those of hexamolybdates as a consequence of one molybdenum atom being substituted by vanadium. The anion cluster skeleton of **VMo_5** demonstrates a slight shrinkage relative to its parent POMs of hexamolybdates after the substitution of a vanadium atom because V^V has a shorter ion radius (0.53 Å) compared to Mo^{VI} (0.59 Å) and short V–O bonds.

Single crystal XRD structural analyses reveal that **V_8Mo_2** ($(TBA)_4[V_8Mo_2O_{28}]$) and **V_9Mo_1** ($(TBA)_4[HV_9MoO_{28}]$) are iso-

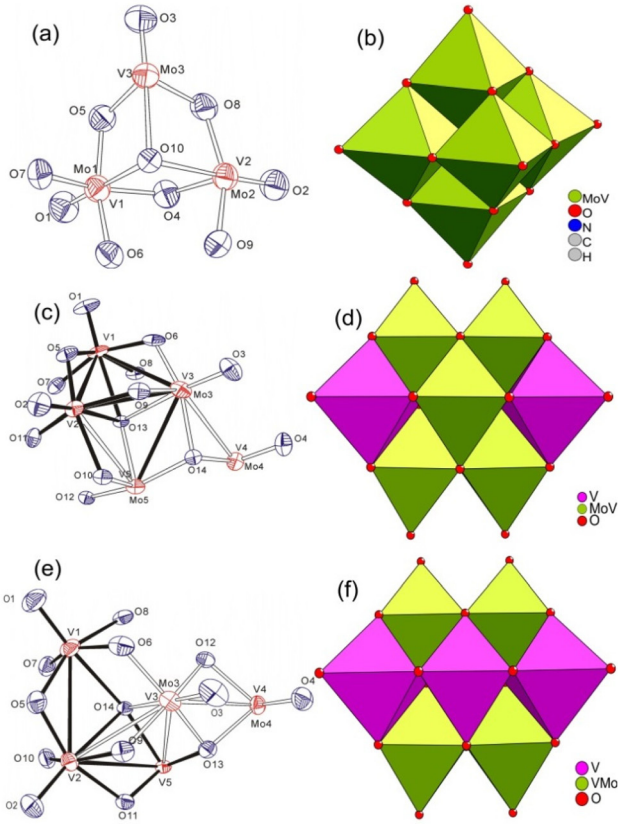

Fig. 1 ORTEP drawing and polyhedron diagram of $[VMo_5O_{19}]^{3-}$ (a and b), $[Mo_2V_8O_{28}]^{4-}$ (c and d), and $[HV_9MoO_{28}]^{4-}$ (e and f).

structural, and both compounds crystallize in the triclinic system, $P\bar{1}$ space group with an anion structure similar to $\mathbf{V_{10}}$. There are two half anion clusters ($[V_8Mo_2O_{28}]^{4-}$ for $\mathbf{V_8Mo_2}$, $[HV_9MoO_{28}]^{4-}$ for $\mathbf{V_9Mo_1}$), four TBA cations and two acetonitrile solvent molecules in their asymmetric unit. As shown in Fig. 1(c and e), the whole anion cluster consisted of two octahedral metal skeleton cages *via* edge-sharing. Both compounds can be viewed as one or two vanadium atoms of the parent decavanadates being substituted by one or two molybdenum atoms. In contrast to the random distribution of vanadium atoms in the anion cluster of $\mathbf{VMo_5}$, the distribution of molybdenum atoms in the anion cluster of $\mathbf{V_8Mo_2}$ and $\mathbf{V_9Mo_1}$ has some preference for some sites. It is well known that there are three kinds of sites in the decavanadate anion cluster according to their coordination environment (as shown in Scheme 1). Two sites A are sited on the common edge of both metal octahedral skeleton and six-coordinated with two μ_2-O_b, two μ_3-O and two μ_6-O atoms; four sites B stand on the equatorial plane with two sites A and are six-coordinated with one terminal O_t, four μ_2-O_b and one μ_6-O atoms; four sites C lay above/below the equatorial plane and are six-coordinated with one terminal O_t, two μ_2-O_b, two μ_3-O and one μ_6-O atom. According to the refinement result of the occupancy ratio with a free variable, site B and site C in $\mathbf{V_8Mo_2}$ resist the substitution of molybdenum and are designated as fully occupied vanadium; sites C were substituted by molybdenum atoms with the occupancy of Mo ranging from 0.19311 to 0.30689. It is notable that the occupancy of molybdenum in sites C (0.19311) for $\mathbf{V_8Mo_2}$ cannot be ignored although it had been thought that only sites B can be substituted by molybdenum atom in other studies.[66] But in $\mathbf{V_9Mo_1}$, only sites B resist the substitution of molybdenum. Sites C (Mo occupancies ranging from 0.37807 to 0.48547) are preferentially substituted by molybdenum compared to sites A (Mo occupancies ranging from 0.13505 to 0.13643). Because the bond lengths of Mo–O are generally longer than that of the corresponding V–O, the bond lengths of M–O in these molybdenum substituted sites are slightly longer than those of V–O bonds (Table S2‡).

Bond valence sum (BVS) is used to judge the oxidation state of metal ions in the title compounds.[67,68] As shown in Table S3,‡ BVS of Mo/V sites in $\mathbf{VMo_5}$ (5.64, 5.75, 5.57 for anion A; 5.71, 5.63, 5.66 for anion B) are close to the theoretical value of 5.83 derived from the random distribution of one vanadium atom in the hexamolybdate cluster. BVS for these sites fully occupied by vanadium in $\mathbf{V_8Mo_2}$ and $\mathbf{V_9Mo_1}$ are all close to 5.0, while BVS for these Mo/V disordered sites in $\mathbf{V_8Mo_2}$ is 5.64, 5.67, 5.65 and 5.60 for sites C, and 5.23 and 5.17 for sites A, which is consistent with the preferential substitution of sites C compared with sites B. BVS for the Mo/V disordered sites in $\mathbf{V_9Mo_1}$ is 5.29, 5.32, 5.31 and 5.20 for sites B, in accordance with the random distribution (5.25) of one vanadium atom at sites C of decavanadates.

Spectral characterization

FT-IR spectra of $\mathbf{VMo_5}$, $\mathbf{V_8Mo_2}$ and $\mathbf{V_9Mo_1}$ are shown in Fig. 2a–c. Generally, the substitution of hexamolybdates by vanadium would split the IR peak of hexamolybdates: one peak shifts to higher wave-numbers because the vanadium atom possesses a smaller ion radius and shorter V–O bond than the molybdenum atom.[61,69] *Vice versa*, the substitution by molybdenum in decavanadates would result in the IR peak shifting to lower wave-numbers. Hexamolybdates, the parent POMs of $\mathbf{VMo_5}$, have a strong peak *ca.* 954 cm^{-1} associated with the stretching vibration of υ(Mo–O_t) and a medium peak *ca.* 750 cm^{-1} ascribed as υ(Mo–O_b).[70] $\mathbf{VMo_5}$ shows a weak peak at 977 cm^{-1}

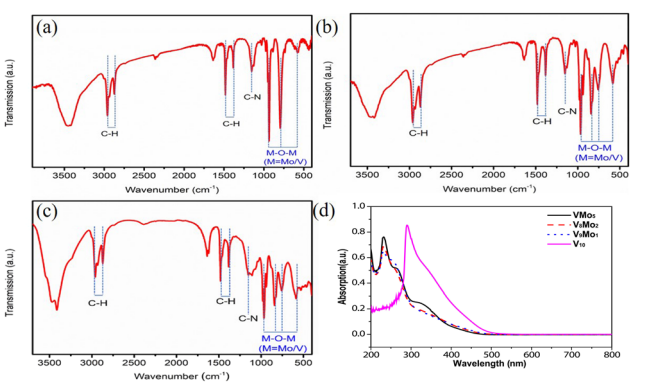

Fig. 2 FT-IR ((a), $\mathbf{VMo_5}$; (b), $\mathbf{V_8Mo_2}$, (c), $\mathbf{V_9Mo_1}$) and UV-Vis (d) spectra of $\mathbf{VMo_5}$, $\mathbf{V_8Mo_2}$ and $\mathbf{V_9Mo_1}$.

attributed to υ(V–O_t) and a stronger peak *ca.* 934 cm^{-1} ascribed to υ(Mo–O_t), indicating the splitting of υ(Mo–O_t) owing to the substitution of vanadium. As for $\mathbf{V_8Mo_2}$ and $\mathbf{V_9Mo_1}$, whose parent POMs of decavanadates have two peaks *ca.* 999 and 957 cm^{-1} associated with υ(V–O_t), are shifted to *ca.* 981 and 938 cm^{-1} in $\mathbf{V_8Mo_2}$ and to *ca.* 966 and 938 cm^{-1} in $\mathbf{V_9Mo_1}$ as a result of one or two vanadium atoms in $\mathbf{V_{10}}$ being substituted by molybdenum atoms.[71]

In the Raman spectra of $\mathbf{VMo_5}$, $\mathbf{V_8Mo_2}$ and $\mathbf{V_9Mo_1}$ (Fig. S1–S3‡), besides the symmetrical and unsymmetrical stretching vibration of methyl and methylene, (2870–2960 cm^{-1}), deformation vibration of methyl (*ca.* 1460 cm^{-1}), the twisting vibration of methylene (*ca.* 1320 cm^{-1}),[72] and the split peak of the stretching vibration of V=O and Mo=O are found at *ca.* 974 and 939 cm^{-1} for $\mathbf{VMo_5}$. The stretching vibration of M=O appeared at *ca.* 986 cm^{-1} for $\mathbf{V_8Mo_2}$ and 993 cm^{-1} for $\mathbf{V_9Mo_1}$.

The electronic absorption spectra of $\mathbf{VMo_5}$, $\mathbf{V_8Mo_2}$ and $\mathbf{V_9Mo_1}$ are studied by UV–Vis spectra in acetonitrile solvent (Fig. 2d) at 230 nm, which are associated with the charge transfer on the multiple bonds of M=O (M = V, Mo). In addition, in the UV-Vis spectra of $\mathbf{VMo_5}$, there is a medium absorption band (331 nm) associated with the charge transfer of the π electrons on the delocalized Lindqvist cluster, which has a slight bathochromic shift compared with the parent hexamolybdate ($\lambda_{max} \approx 324$ nm) owing to the substitution of the vanadium atom.[69] As for $\mathbf{V_8Mo_2}$ and $\mathbf{V_9Mo_1}$, the electronic transition of π electrons on the anion skeleton appears at 352 and 347 nm with some bathochromic shifts compared to decavanadates, owing to the substitution of vanadium by the molybdenum atom in the structure of $\mathbf{V_8Mo_2}$ and $\mathbf{V_9Mo_1}$.

The high resolution mass spectra (HR MS) of $\mathbf{VMo_5}$, $\mathbf{V_8Mo_2}$ and $\mathbf{V_9Mo_1}$ are shown in Fig. S4–S9.‡ In the positive region, there are two major positive ion peaks of $\mathbf{VMo_5}$: one peak about m/z = 1561.2429 is well matched with $[M + H]^+$ (calcd: 1561.2394) and another peak around m/z = 1802.5153 can be ascribed as the cation of $[M + TBA]^+$ (calcd: 1802.5169). Three ion peaks are found in the HR MS of $\mathbf{V_8Mo_2}$: the peak *ca.* 2261.6505 is associated with $[M + TBA]^+$ (calcd. 2261.6475), the peak centered at 2019.3696 is associated with $[M + H]^+$ (calcd. 2019.3693), and the strongest ion peak of 1251.9697 is well matched with $[M + 2TBA]^{2+}$ (calcd. 1251.9697). Similarly, there are three molecular ion peaks for the positive pattern in the HR MS of $\mathbf{V_9Mo_1}$. The peak at *ca.* 1975.3902 is well matched with $[M + H]^+$ (calcd. 1975.4149), the molecular ion peak of $[M + TBA]^+$ (calcd. 2216.7005) is found *ca.* 2216.6776, and the molecular peak at *ca.* 1229.4815 is attributed to $[M + 2TBA]^{2+}$ (calcd: 1229.1961).

X-ray photoelectron spectroscopy (XPS) was performed to further confirm the composition and oxidation state. The XPS spectra of $\mathbf{V_1Mo_5}$, $\mathbf{V_8Mo_2}$ and $\mathbf{V_9Mo_1}$ reveal the presence of C, N, O, Mo and V. The narrow XPS spectra (Fig. S10–S12‡) show the characteristic Mo(3d) doublet ($Mo_{3d3/2}$, $Mo_{3d5/2}$) around *ca.* 232.1, 235.3 eV for $\mathbf{VMo_5}$, 232.2 eV, 235.3 eV for $\mathbf{V_8Mo_2}$, and 232.3, 235.5 eV for $\mathbf{V_9Mo_1}$, in agreement with the literature values of molybdenum(VI) (231.3 eV, 235.8 eV).[73,74] The doublet of V(2p) ($V_{2p1/2}$, $V_{2p3/2}$) is found at *ca.* 516.6, 524.1 eV in $\mathbf{V_1Mo_5}$, 516.4, 523.9 eV in $\mathbf{V_8Mo_2}$, 517.0, 524.2 eV in $\mathbf{V_9Mo_1}$, respectively, in accordance with the literature values of vanadium(V) (517.0 eV, 524.2 eV).[73,75] The XPS results confirm the presence of molybdenum and vanadium and their oxidation state as +6 and +5, respectively. This is consistent with the results of the crystal structure analysis and BVS. To further validate their composition, inductively coupled plasma emission spectroscopy (ICP-MS) was conducted to determine the atomic ratio of vanadium and molybdenum atom in the title compounds. ICP-MS results indicate that the V/Mo atomic ratio in $\mathbf{VMo_5}$, $\mathbf{V_8Mo_2}$ and $\mathbf{V_9Mo_1}$ is 0.20 (1 : 5), 4.00 (4 : 1) and 9.25 (9 : 1), respectively, in agreement with the results of single crystal structure analysis.

Diffuse reflection spectra were measured to obtain the band gap (E_g) of the title compounds. E_g was determined as the intersection point between the energy axis and the line extrapolated from the linear portion of the absorption edge in a plot of the Kubelka–Munk function F against energy E. The Kubelka–Munk function, $F = (1 - R)^2/2R$, was converted from the recorded diffuse reflectance data, where R is the reflectance of an infinitely thick layer at a given wavelength.[70,76,77] On the F *versus* E plot (Fig. 3), a steep absorption edge is displayed from which the E_g of $\mathbf{V_1Mo_5}$, $\mathbf{V_8Mo_2}$, $\mathbf{V_9Mo_1}$ and $\mathbf{V_{10}}$ can be assessed at 2.47 eV, 2.42 eV, 2.36 eV and 2.31 eV, respectively. This means that the bandgap of the title compounds can also be tuned by the substitution of addenda atom of POMs.

Nonlinear optical properties

In view of these compounds possessing delocalized π electrons in their cluster skeletons, we decided to explore their third-order NLO properties.

$\mathbf{V_1Mo_5}$, $\mathbf{V_8Mo_2}$ and $\mathbf{V_9Mo_1}$ can be dispersed into nano particles in *n*-hexane solvent *via* ultrasonication (10–15 min). The samples for SEM and TEM are prepared through dropping their suspensions on a single polished silicon wafer and copper net (200 mesh), respectively, and those silicon wafers and copper nets are vacuum dried after the evaporation of the solvent.

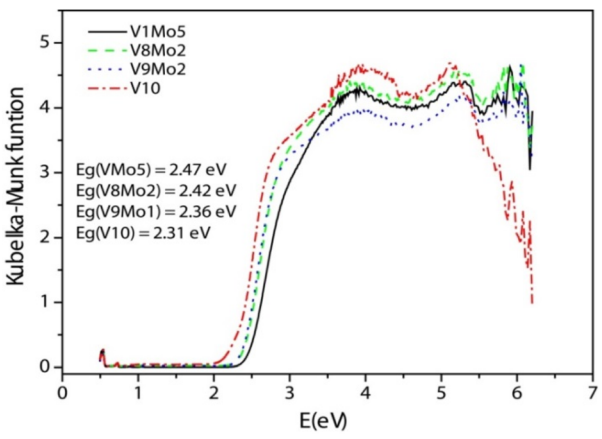

Fig. 3 Solid UV-Vis reflection spectra of $\mathbf{VMo_5}$, $\mathbf{V_8Mo_2}$, $\mathbf{V_9Mo_1}$ and $\mathbf{V_{10}}$.

According to the results of SEM (Fig. S13‡), TEM and HAADF (Fig. 4 and 5 and Fig. S14‡), their sizes and morphologies are not uniform: the particle size of $\mathbf{V_1Mo_5}$ varies from 300 nm to 1700 nm, the particle size of $\mathbf{V_8Mo_2}$ ranges from 400 nm to 1500 nm, and the particle size of $\mathbf{V_9Mo_1}$ changes from 300 nm to 1000 nm. The energy dispersive X-ray spectroscopy (EDX) mapping images of $\mathbf{V_1Mo_5}$, $\mathbf{V_8Mo_2}$ and $\mathbf{V_9Mo_1}$ show the presence of V and Mo elements in those compounds. In their composite image of V/Mo, $\mathbf{V_8Mo_2}$ and $\mathbf{V_9Mo_1}$ possess more vanadium than molybdenum, but $\mathbf{V_1Mo_5}$ has less vanadium than molybdenum.

All samples for the solution NLO test are first dispersed in propanetriol to form a suspension with a transmittance *ca.* 65–75%. The NLO properties of $\mathbf{V_{10}}$, $\mathbf{V_1Mo_5}$, $\mathbf{V_8Mo_2}$ and $\mathbf{V_9Mo_1}$ were investigated using the *Z*-scan technique[78] on a nanosecond laser at the wavelengths of 532 nm and 1064 nm, respectively.

As shown in Fig. 6(a and c), the *Z*-scan curves of all compounds in an open aperture configuration display a transmittance valley for both lasers at 532 and 1064 nm, which means a typical nonlinear absorption.[1] Upon laser irradiation of

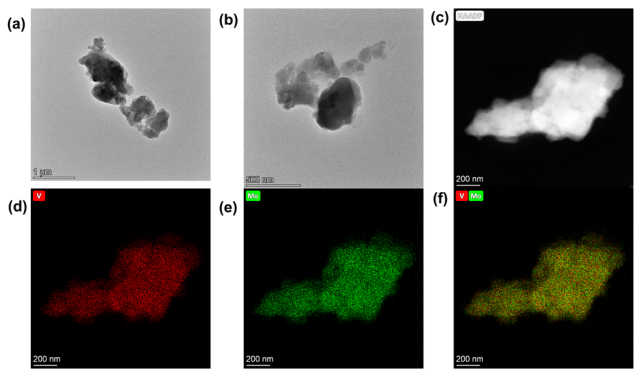

Fig. 4 TEM images of $\mathbf{V_1Mo_5}$: (a) and (b) TEM images, (c) HAADF-STEM image; (d,e) corresponding EDX mapping of V and Mo distribution; (f) composite of V/Mo.

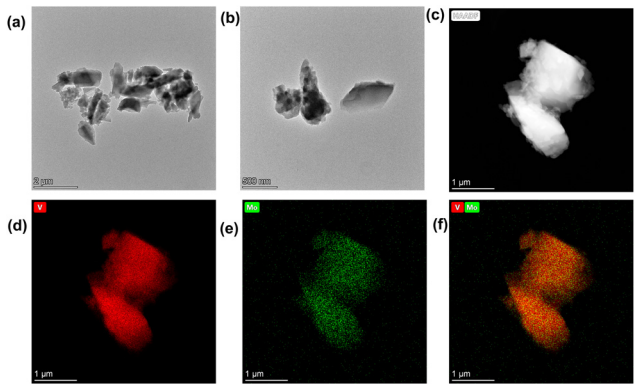

Fig. 5 TEM images of $\mathbf{V_9Mo_1}$: (a) and (b) TEM images, (c) HAADF-STEM image; (d) corresponding EDX mapping of V and Mo distribution; (f) composite of V/Mo.

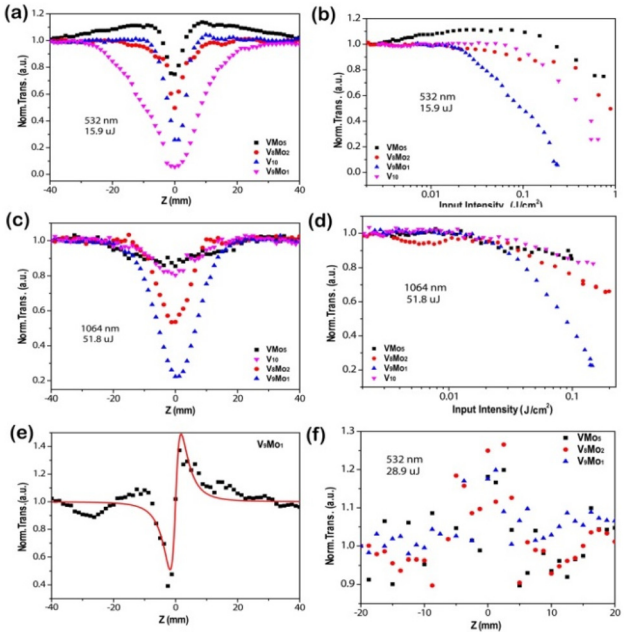

Fig. 6 *Z*-Scan nonlinear absorption results (a and c), transmittance *vs.* incident intensity (b and d), and nonlinear scattering results (f) of the glycerol suspensions of polyoxomolybdovanadates at 532 and 1064 nm; *Z*-scan non-linear refraction of $\mathbf{V_9Mo_1}$ at 532 nm (e).

532 nm with a pulse energy of 15.9 μJ, T_{min} was about 0.75 for $\mathbf{V_1Mo_5}$, 0.50 for $\mathbf{V_8Mo_2}$, 0.06 for $\mathbf{V_9Mo_1}$ and 0.26 for $\mathbf{V_{10}}$, respectively. And T_{min} was about 0.85 for $\mathbf{V_1Mo_5}$, 0.53 for $\mathbf{V_8Mo_2}$, 0.22 for $\mathbf{V_9Mo_1}$ and 0.80 for $\mathbf{V_{10}}$ for laser irradiation at 1064 nm with a pulse energy of 51.8 μJ. The small T_{min} and broad valley width in the *Z*-scan curves of $\mathbf{V_{10}}$, $\mathbf{V_8Mo_2}$ and $\mathbf{V_9Mo_1}$ mean that they are better candidates for NLO materials compared to $\mathbf{V_1Mo_5}$, possibly because they possess a large delocalized π electron system. $\mathbf{V_9Mo_1}$ in particular exhibits the smallest transmittance and the biggest valley width at both wavelengths. The closed aperture *Z*-scan results of the title compounds were obtained to detect their nonlinear refraction. As shown in Fig. 6(e) and Fig. S14,‡ there is a valley–peak pattern in their closed aperture *Z*-scan curves, implying the positive sign of the refractive nonlinearity and the self-focusing effect of $\mathbf{V_9Mo_1}$. In addition, the nonlinear scattering signals of the title compounds irradiated by the 532 nm laser were collected when the detector was put in the direction with a deviation of 5° from the laser beam (Fig. 6f). The scattering of peaks of all compounds relative to the focal point can be observed in their suspensions. Therefore, the third-order NLO properties of the title compounds combined NLA and NLS with NLR, which enhanced their NLO response efficiently. A plot of normalized transmittance *versus* input fluence is presented in Fig. 6(b and d), in which the optical energy-limiting onset fluence (F_{on}) is defined as the fluence where transmittance starts to fall to 95% of its original value.[79,80] Upon incident laser irradiation of 532 nm, the F_{on} values of $\mathbf{V_1Mo_5}$, $\mathbf{V_8Mo_2}$, $\mathbf{V_9Mo_1}$ and $\mathbf{V_{10}}$ are 230, 38, 22 and 84 mJ cm^2, respect-

Table 1 NLO coefficients of V_{10}, V_1Mo_5, V_8Mo_2 and V_9Mo_1 suspensions under laser irradiation of 532 and 1064 nm

Compounds	Λ [nm]	T_{min}	β_{eff} [cm GW^{-1}]	Im $\chi^{(3)}$ [esu]	n_2
V_1Mo_5	532	0.75	60.16	2.9×10^{-8}	1.08×10^{-5}
V_8Mo_2		0.50	123.79	6.0×10^{-8}	8.9×10^{-6}
V_9Mo_1		0.06	691.79	3.3×10^{-7}	9.95×10^{-6}
V_{10}		0.26	202.63	9.8×10^{-8}	
V_1Mo_5	1064	0.85	80.19	7.8×10^{-8}	
V_8Mo_2		0.53	127.98	1.24×10^{-7}	
V_9Mo_1		0.22	292.52	2.8×10^{-7}	
V_{10}		0.80	69.59	6.8×10^{-8}	

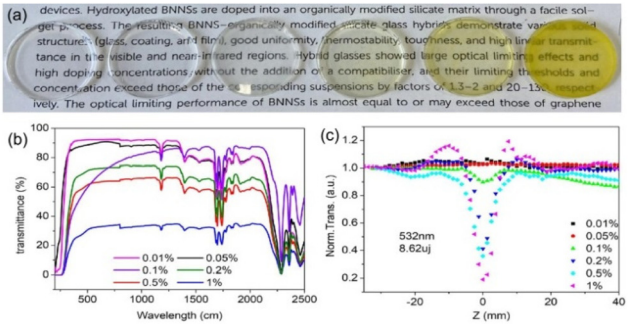

Fig. 7 Photographs, transmittance spectra and *Z*-scan results of those hybrid gel glasses with different doping level of V_9Mo_1: (a) photograph of those hybrid gel glasses; (b) transmittance spectra of hybrid gel glasses; (c) open aperture *Z*-scan results of hybrid gel glasses for the laser of 532 nm.

ively; for the laser of 1064 nm, their F_{on} values are 16, 15, 20, and 16 mJ cm^2, respectively. V_9Mo_1 has the lowest F_{on} values for the lasers at both wavelengths, implying its better NLO properties.

The nonlinear absorption coefficient β_{eff} and the imaginary part of the third-order NLO susceptibility Im $\chi^{(3)}$ of the title compounds (Table 1) were obtained through fitting their NLA curves.[78,81] The calculated β_{eff} values of V_{10}, V_1Mo_5, V_8Mo_2 and V_9Mo_1 by the NLA curves for the 532 nm laser are 202.63 cm GW^{-1}, 60.16 cm GW^{-1}, 123.79 cm GW^{-1} and 691.79 cm GW^{-1}, respectively. According to the NLA curves obtained for the 1064 nm laser, the calculated β_{eff} values for V_{10}, V_1Mo_5, V_8Mo_2 and V_9Mo_1 are 69.59 cm GW^{-1}, 80.19 cm GW^{-1}, 127.98 cm GW^{-1} and 292.52 cm GW^{-1}, respectively. Similarly, their Im $\chi^{(3)}$ values can be obtained for V_{10} (9.8×10^{-8} esu at 532 nm, 6.8×10^{-8} esu at 1064 nm), V_1Mo_5 (2.9×10^{-8} esu at 532 nm, 7.8×10^{-8} esu at 1064 nm), V_8Mo_2 (6.0×10^{-8} esu at 532 nm, 1.24×10^{-7} esu at 1064 nm) and V_9Mo_1 (3.3×10^{-7} esu at 532 nm, 2.8×10^{-7} esu at 1064 nm) by fitting their NLA curves. Therefore, V_9Mo_1 has the largest nonlinear absorption coefficient β_{eff} and the imaginary part of the third-order NLO susceptibility Im $\chi^{(3)}$ upon laser irradiation at both wavelengths, meaning that V_9Mo_1 is the best candidates for OL materials in these compounds.

Given the excellent NLO property of V_9Mo_1, it was chosen to be doped into the matrix of ORMOSIL gel glasses to further investigate its NLO and OL properties. V_9Mo_1-doped gel glasses were prepared through putting the finely ground samples into the pre-prepared gel which was obtained by the hydrolysis and polycondensation reaction of methyltriethoxysilane (MTES). Photos of V_9Mo_1-doped gel glasses with different doping levels (0.01 wt%–1 wt%) are shown in Fig. 7(a). It can be seen that these gel glasses have a smooth surface without cracks and can be directly used for further optical measurement. From the low doping level (0.01 wt%–0.1 wt%) to the medium doping level (0.5%), all gel glass hybrids of V_9Mo_1 still maintain an excellent transparence. However, when the doping level rises up to a high level (1.0%), the gel glass becomes opaque to some extent possibly due to the aggregation of V_9Mo_1. Their transmission spectra (Fig. 7b) show that the linear transmittance of these V_9Mo_1-doped gel glass reduced from 80% to 30–40% gradually accompanied by the increase of the doping level of V_9Mo_1 from 0.01 wt% to 1.0 wt%. The *Z*-scan results of V_9Mo_1-doped gel glasses upon laser irradiation at 532 nm with the pulse energy of 8.62 μJ are shown in Fig. 7(c). It can be seen that V_9Mo_1 in the solid matrix of gel glass still maintained a NLA response similar to that observed in its suspension in propanetriol. In addition, the NLA response of V_9Mo_1-doped gel glass hybrids with a low doping level of 0.01% and 0.05% is very weak, but it enhanced gradually with the increasing modulation depth along with the increase of doping level in the gel glasses. Moreover, the normalized absorption T_{min} dropped to 19.1% at the doping level of 1 wt%. Therefore, V_9Mo_1-doped gel glasses demonstrate a concentration-dependent NLA response.

OL behaviors of gel glass hybrids were studied using the lasers with different wavelengths of 532, 1064 and 2150 nm. The curves of output influence *versus* incident fluence of those gel glass hybrids are plotted in Fig. 8. The blank gel glass at 532 nm and 1064 nm has no OL response because its output fluence increases linearly at both low input fluence and high input fluence. These gel glass hybrids with a low doping level (0.01 wt% and 0.05 wt%) of V_9Mo_1 exhibit a very weak OL effect owing to their weak NLA. But the gel glass hybrids with a medium to high doping level (0.1%, 0.2%, 0.5%, 1.0 wt%) of V_9Mo_1 demonstrate obvious OL behavior along with an increase of the doping level of V_9Mo_1 because their output influence increases linearly at low influence but deviated from linearity at high influence. And 1.0 wt% V_9Mo_1-doped gel glass with the highest doping concentration exhibits the strongest OL ability. The optical limiting threshold (F_{on}) of the V_9Mo_1-doped gel glasses upon the irradiation of a 532 nm laser was 2.51 J cm^{-2} for 0.01%, 1.22 J cm^{-2} for 0.02%, 1.29 J cm^{-2} for 0.05%, and 1.22 J cm^{-2} for 1%, respectively. Under the irradiation of the laser at 1064 nm, the optical limiting threshold (F_{on}) of gel glasses was 2.92 J cm^{-2} for 0.01%, 1.12 J cm^{-2} for 0.02%, 0.91 J cm^{-2} for 0.05%, 0.67 J cm^{-2} for 1%, respectively. Therefore, the OL ability of these gel glasses can be modulated easily by controlling the doping level of V_9Mo_1. Moreover, OL behaviors of these gel glass hybrids are also observed for the laser of 2150 nm, indicating that these gel

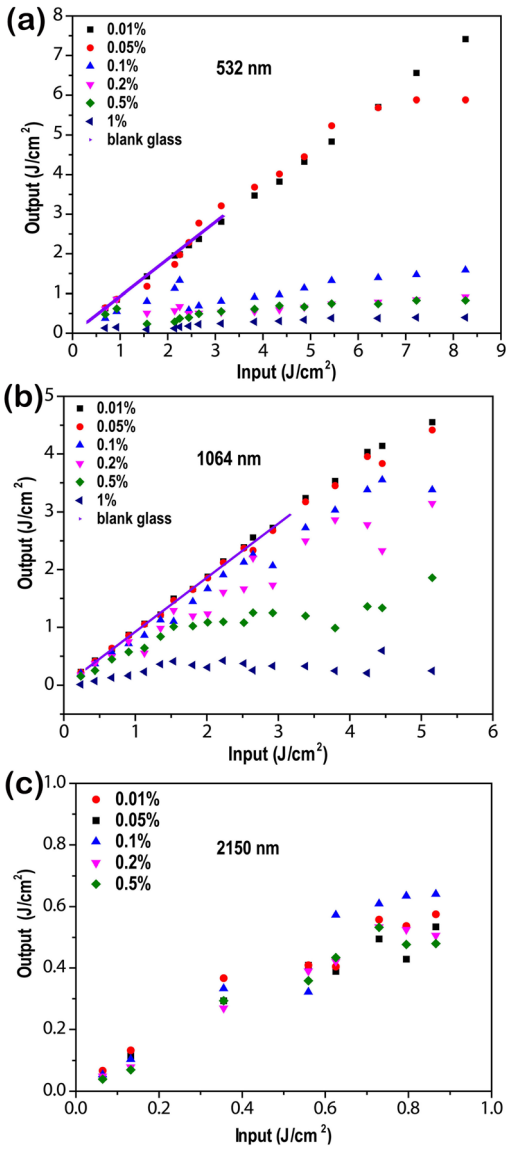

Fig. 8 OL behaviors of gel glass hybrids containing 0.01, 0.05, 0.1, 0.2, 0.5, and 1.0 wt% $\mathbf{V_9Mo_1}$ at the laser of 532 nm (a), 1064 nm (b) and 2150 nm (c).

glasses are a class of broadband solid-state optical limiters. To the best of our knowledge, this is the first example of superbroadband optical limiter based on crystalline metal cluster compounds.

Conclusions

In summary, we have developed a general procedure of acidification–precipitation–crystallization to afford polyoxomolybdovanadates including $[TBA]_3[VMo_5O_{19}]$ ($\mathbf{V_1Mo_5}$), $[TBA]_4[V_8Mo_2O_{28}]$ ($\mathbf{V_8Mo_2}$) and $[TBA]_4[HV_9MoO_{28}]$ ($\mathbf{V_9Mo_1}$) in modest to high yields. Single crystal X-ray diffraction structural analysis reveals that $\mathbf{V_1Mo_5}$ demonstrates a typical Lindqvist structure with a random distribution of the vanadium atoms in the anion cluster. Although $\mathbf{V_8Mo_2}$ and $\mathbf{V_9Mo_1}$ exhibit a decavanadate-like structure, the distribution of molybdenum atoms in their anion clusters is not random. Their band gaps and NLO properties are tuned by the substitution of addenda atoms in hexamolybdates or decavanadates. According to the structural type of POMs, $\mathbf{V_9Mo_1}$ is the best candidate for optical limiting materials due to its smallest transmittance, biggest valley width, largest nonlinear absorption coefficient β_{eff} and the imaginary part of the third-order NLO susceptibility Im $\chi^{(3)}$ in all compounds. A series of ORMOSIL gel glass hybrids with different doping levels (from 0.01% to 1 wt%) of $\mathbf{V_9Mo_1}$ was prepared. Moreover, those gel glass hybrids with medium to high doping levels of $\mathbf{V_9Mo_1}$ display obvious optical limiting behavior for lasers of 532 nm, 1064 nm and 2150 nm, which become strong gradually along with the increase of the $\mathbf{V_9Mo_1}$ concentration. Our current research not only puts forward a simple strategy to modulate the third-order NLO responses of POMs through the substitution of the addenda metal atoms in POMs, but also provides several polyoxomolybdovanadates as potential NLO materials, especially $\mathbf{V_9Mo_1}$, which represents the first example of a superbroadband optical limiter in the visible and long-wavelength near-infrared regions based on crystalline metal cluster compounds so far. Moreover, the successful preparation of POM-doped gel glass would pave the way of POMs as NLO materials in the applications of diverse optical devices.

Conflicts of interest

There are no conflicts to declare.

Acknowledgements

We are thankful for the financial support of the National Natural Science Foundation of China (21101062), Science and Technology Department of Hubei Province (2014CFB600), Youth Chutian Scholar Fund of Hubei Province (4032401), State Key Laboratory of Structural Chemistry (20180023), Key Laboratory of Photochemical Conversion and Optoelectronic Materials, TIPC, CAS. (PCOM 202216) and Hubei Provincial Key Laboratory of Green Materials for Light Industry (201710A11, 201907A09).

Notes and references

1 D. Dini, M. J. Calvete and M. Hanack, Nonlinear Optical Materials for the Smart Filtering of Optical Radiation, *Chem. Rev.*, 2016, **116**, 13043–13233.
2 W. Nie, Optical Nonlinearity: Phenomena, Applications, and Materials, *Adv. Mater.*, 1993, **5**, 520–545.
3 L. W. Tutt and T. F. Boggess, A Review of Optical Limiting Mechanisms and Devices Using Organics, Fullerenes, Semiconductors and Other Materials, *Prog. Quantum Electron.*, 1993, **17**, 299–338.
4 F. Hache, D. Ricard, C. Flytzanis and U. Kreibig, The Optical Kerr Effect in Small Metal Particles and Metal

Colloids: The Case of Gold, *Appl. Phys. A*, 1988, **47**, 347–357.

5 G. Li, S. Zhang and T. Zentgraf, Nonlinear photonic metasurfaces, *Nat. Rev. Mater.*, 2017, **2**, 17010, DOI: **10.1038/natrevmats.2017.10**.

6 L. Wu, Y. Dong, J. Zhao, D. Ma, W. Huang, Y. Zhang, Y. Wang, X. Jiang, Y. Xiang, J. Li, Y. Feng, J. Xu and H. Zhang, Kerr Nonlinearity in 2D Graphdiyne for Passive Photonic Diodes, *Adv. Mater.*, 2019, **31**, 1807981, DOI: **10.1002/adma.201807981**.

7 L. Wu, Z. Xie, L. Lu, J. Zhao, Y. Wang, X. Jiang, Y. Ge, F. Zhang, S. Lu, Z. Guo, J. Liu, Y. Xiang, S. Xu, J. Li, D. Fan and H. Zhang, Few-Layer Tin Sulfide: A Promising Black-Phosphorus-Analogue 2D Material with Exceptionally Large Nonlinear Optical Response, High Stability, and Applications in All-Optical Switching and Wavelength Conversion, *Adv. Opt. Mater.*, 2018, **6**, 1700985, DOI: **10.1002/adom.201700985**.

8 L. Lu, W. Wang, L. Wu, X. Jiang, Y. Xiang, J. Li, D. Fan and H. Zhang, All-Optical Switching of Two Continuous Waves in Few Layer Bismuthene Based on Spatial Cross-Phase Modulation, *ACS Photonics*, 2017, **4**, 2852–2861.

9 J. W. You, S. R. Bongu, Q. Bao and N. C. Panoiu, Nonlinear optical properties and applications of 2D materials: theoretical and experimental aspects, *Nanophotonics*, 2018, **8**, 63–97.

10 G.-K. Lim, Z.-L. Chen, J. Clark, R. G. S. Goh, W.-H. Ng, H.-W. Tan, R. H. Friend, P. K. H. Ho and L.-L. Chua, Giant broadband nonlinear optical absorption response in dispersed graphene single sheets, *Nat. Photonics*, 2011, **5**, 554–560.

11 Y. Chen, T. Bai, N. Dong, F. Fan, S. Zhang, X. Zhuang, J. Sun, B. Zhang, X. Zhang, J. Wang and W. J. Blau, Graphene and its derivatives for laser protection, *Prog. Mater. Sci.*, 2016, **84**, 118–157.

12 X. Sun, X. Hu, J. Sun, Z. Xie, S. Zhou and P. Chen, Broadband optical limiting and nonlinear optical graphene oxide co-polymerization Ormosil glasses, *Adv. Compos. Hybrid Mater.*, 2018, **1**, 397–403.

13 Y.-P. He, G.-H. Chen, D.-J. Li, Q.-H. Li, L. Zhang and J. Zhang, Combining a Titanium–Organic Cage and a Hydrogen-Bonded Organic Cage for Highly Effective Third-Order Nonlinear Optics, *Angew. Chem., Int. Ed.*, 2021, **60**, 2920–2923.

14 W. Bi, N. Louvain, N. Mercier, J. Luc, I. Rau, F. Kajzar and B. Sahraoui, A Switchable NLO Organic-Inorganic Compound Based on Conformationally Chiral Disulfide Molecules and Bi(III)I5 Iodobismuthate Networks, *Adv. Mater.*, 2008, **20**, 1013–1017.

15 X.-T. Wu, Q. Huang, Q.-M. Wang, T.-L. Sheng and J.-X. Lu, *New Aspects of Heterometallic Copper (Silver) Cluster Compounds Involving Sulfido Ligands*, American Chemical Society, Washington, DC, 1996.

16 X.-T. Wu, Q.-M. Wang and S. Shi, Optical non-linearity of distorted cubic cageshaped cluster compounds $\{MAg_3S_3[S_2P(OCH_2CH_3)_2]\}(S)(Ph_3P)_3$ (M = W, Mo), *Polyhedron*, 1997, **16**, 945–948.

17 W.-H. Zhang, Q. Liu and J.-P. Lang, Heterometallic transition metal clusters and cluster-supported coordination polymers derived from Tp- and Tp*-based Mo(W) sulfido precursors, *Coord. Chem. Rev.*, 2015, **293**, 187–210.

18 Y.-J. Liu, Q.-H. Li, D.-J. Li, X.-Z. Zhang, W.-H. Fang and J. Zhang, Designable Al32-Oxo Clusters with Hydrotalcite-like Structures: Snapshots of Boundary Hydrolysis and Optical Limiting, *Angew. Chem., Int. Ed.*, 2021, **60**, 2–8.

19 C. L. Hill, *Polyoxometalates - Multicomponent molecular vehicles to probe fundamental issues and practical problems*, American Chemical Society, 1998.

20 R. v. Eldik and L. Cronin, *Polyoxometalate Chemistry*, Academic Press, San Diego, Oxford, London, 2017.

21 P. Yin, D. Li and T. Liu, Counterion Interaction and Association in Metal-Oxide Cluster Macroanionic Solutions and the Consequent Self-Assembly, *Isr. J. Chem.*, 2011, **51**, 191–204.

22 A. Proust, R. Thouvenot and P. Gouzerh, Functionalization of polyoxometalates: towards advanced applications in catalysis and materials science, *Chem. Commun.*, 2008, 1837–1852.

23 Y. Gu, Q. Li, D. Zang, Y. Huang, H. Yu and Y. Wei, Light-Induced Efficient Hydroxylation of Benzene to Phenol by Quinolinium and Polyoxovanadate-Based Supramolecular Catalysts, *Angew. Chem., Int. Ed.*, 2021, **60**, 13310–13316.

24 S. Han, Y. Cheng, S. Liu, C. Tao, A. Wang, W. Wei, H. Yu and Y. Wei, Selective Oxidation of Anilines to Azobenzenes and Azoxybenzenes by a Molecular Mo Oxide Catalyst, *Angew. Chem., Int. Ed.*, 2021, **60**, 6382–6385.

25 S.-S. Wang and G.-Y. Yang, Recent Advances in Polyoxometalate-Catalyzed Reactions, *Chem. Rev.*, 2015, **115**, 4893–4962.

26 F. Xiao, J. Hao, J. Zhang, C. Lv, P. Yin, L. Wang and Y. Wei, Polyoxometalatocyclophanes: Controlled Assembly of Polyoxometalate-Based Chiral Metallamacrocycles from Achiral Building Blocks, *J. Am. Chem. Soc.*, 2010, **132**, 5956–5957.

27 J. Zhang, J. Hao, Y. Wei, F. Xiao, P. Yin and L. Wang, Nanoscale Chiral Rod-like Molecular Triads Assembled from Achiral Polyoxometalates, *J. Am. Chem. Soc.*, 2010, **132**, 14–15.

28 H. Q. Tan, Y. G. Li, Z. M. Zhang, C. Qin, X. L. Wang, E. B. Wang and Z. M. Su, Chiral polyoxometalate-induced enantiomerically 3D architectures: A new route for synthesis of high-dimensional chiral compounds, *J. Am. Chem. Soc.*, 2007, **129**, 10066–10067.

29 Q. Yin, J. M. Tan, C. Besson, Y. V. Geletii, D. G. Musaev, A. E. Kuznetsov, Z. Luo, K. I. Hardcastle and C. L. Hill, A Fast Soluble Carbon-Free Molecular Water Oxidation Catalyst Based on Abundant Metals, *Science*, 2010, **328**, 342–345.

30 W. Xu, X. Pei, C. S. Diercks, H. Lyu, Z. Ji and O. M. Yaghi, A Metal-Organic Framework of Organic Vertices and Polyoxometalate Linkers as a Solid-State Electrolyte, *J. Am. Chem. Soc.*, 2019, **141**, 17522–17526.

31 X. X. Li, Y. X. Wang, R. H. Wang, C. Y. Cui, C. B. Tian and G. Y. Yang, Designed assembly of heterometallic cluster

organic frameworks based on anderson-type polyoxometalate clusters, *Angew. Chem., Int. Ed.*, 2016, **55**, 6462–6466.

32 X. Kuang, X. Wu, R. Yu, J. P. Donahue, J. Huang and C.-Z. Lu, Assembly of a metal–organic framework by sextuple intercatenation of discrete adamantane-like cages, *Nat. Chem.*, 2010, **2**, 461–465.

33 T. Liu, E. Diemann, H. Li, A. W. M. Dress and A. Mueller, Self-assembly in aqueous solution of wheel-shaped Mo154 oxide clusters into vesicles, *Nature*, 2003, **426**, 59–62.

34 T. Liu, M. L. K. Langston, D. Li, J. M. Pigga, C. Pichon, A. M. Todea and A. Mueller, Self-Recognition Among Different Polyprotic Macroions During Assembly Processes in Dilute Solution, *Science*, 2011, **331**, 1590–1592.

35 X. Lopez, J. J. Carbo, C. Bo and J. M. Poblet, Structure, properties and reactivity of polyoxometalates: a theoretical perspective, *Chem. Soc. Rev.*, 2012, **41**, 7537–7571.

36 T. Zhang, W. Guan, T. Ma, Y. Lin, L. Yan and Z. Su, Theoretical studies on tricarbonyl metal derivatives of Lindqvist-type polyoxometalate complexes: electronic structures and nonlinear optical properties, *Inorg. Chem. Front.*, 2015, **2**, 544–549.

37 T. Zhang, L.-K. Yan, S. Cong, W. Guan and Z.-M. Su, Prediction of second-order nonlinear optical properties of Wells–Dawson polyoxometalate derivatives $[X\text{–}C(CH_2O)_3P_2M'_3M_{15}O_{59}]^{6-}$ (X = NO_2, NH_2, and CH_3, M′ = V and Nb, M = W and Mo), *Inorg. Chem. Front.*, 2014, **1**, 65–70.

38 J.-y. Niu, X.-z. You and C.-y. Duan, A Novel Optical Complex between an Organic Substrate and a Polyoxometalate. Crystal and Molecular Structure of α-$H4SiW_{12}O_{40}$·4HMPA·$2H_2O$ (HMPA = Hexamethylphosphoramide), *Inorg. Chem.*, 1996, **35**, 4211–4217.

39 W. W. Ju, H. T. Zhang, X. Xu, Y. Zhang and Y. Xu, Enantiomerically pure lanthanide-organic polytungstates exhibiting two-photon absorption properties, *Inorg. Chem.*, 2014, **53**, 3269–3271.

40 M. O. Senge, M. Fazekas, E. G. A. Notaras, W. J. Blau, M. Zawadzka, O. B. Locos and E. M. Ni Mhuircheartaigh, Nonlinear Optical Properties of Porphyrins, *Adv. Mater.*, 2007, **19**, 2737–2774.

41 L. Zhang and L. Wang, Recent research progress on optical limiting property of materials based on phthalocyanine, its derivatives, and carbon nanotubes, *J. Mater. Sci.*, 2008, **43**, 5692–5701.

42 F. K. Shehzad, A. Iqbal, Y. Zhou, L. Zhang, T. Wang and X. Ren, Organic–Inorganic Hybrids Composed of Keggin-Type $[PMo_{10}V_2O_{40}]^{5-}$ Anions and Porphyrins: The Synthesis, Characterization, and Influence of Porphyrin Substituents on Optical Nonlinearities, *J. Phys. Chem. C*, 2020, **124**, 9442–9450.

43 H. M. Asif, N. Qu, Y. Zhou, L. Zhang, F. K. Shehzad, Z. Shi, Y. Long and S. U. Hassan, Third-order NLO properties of ultrathin films containing cationic phthalocyanine and Keggin polyoxometalates fabricated using layer-by-layer deposition from aqueous solution, *Inorg. Chem. Front.*, 2017, **4**, 1900–1908.

44 A. Iqbal, H. M. Asif, Y. Zhou, L. Zhang, T. Wang, F. K. Shehzad and X. Ren, From Simplicity to Complexity in Grafting Dawson-Type Polyoxometalates on Porphyrin, Leading to the Formation of New Organic-Inorganic Hybrids for the Investigation of Third-Order Optical Nonlinearities, *Inorg. Chem.*, 2019, **58**, 8763–8774.

45 S. u. Hassan, H. M. Asif, Y. Zhou, L. Zhang, N. Qu, J. Li and Z. Shi, "Closer is Better and Two is Superior to One": Third-Order Optical Nonlinearities of a Family of Porphyrin–Anderson Type Polyoxometalate Hybrid Compounds, *J. Phys. Chem. C*, 2016, **120**, 27587–27599.

46 A. Boulmier, A. Vacher, D. Zang, S. Yang, A. Saad, J. Marrot, O. Oms, P. Mialane, I. Ledoux, L. Ruhlmann, D. Lorcy and A. Dolbecq, Anderson-Type Polyoxometalates Functionalized by Tetrathiafulvalene Groups: Synthesis, Electrochemical Studies, and NLO Properties, *Inorg. Chem.*, 2018, **57**, 3742–3752.

47 X. M. Liu, F. Q. Meng, W. W. Cheng, J. P. Cao, J. L. Wang, T. T. Zang, Q. D. Ping, H. Xie and Y. Xu, Two new isolated Zn-epsilon-Keggin clusters modified by conjugated organic ligands with decent electrocatalytic and third-order NLO properties, *Dalton Trans.*, 2020, **49**, 14251–14257.

48 X. M. Luo, N. F. Li, Z. B. Hu, J. P. Cao, C. H. Cui, Q. F. Lin and Y. Xu, Polyoxometalate-Based Well-Defined Rodlike Structural Multifunctional Materials: Synthesis, Structure, and Properties, *Inorg. Chem.*, 2019, **58**, 2463–2470.

49 F. Xing, J. Wang, Z. Wang, Y. Li, X. Gou, H. Zhang, S. Zhou, J. Zhao and Z. Xie, Covalently Silane-Functionalized Antimonene Nanosheets and Their Copolymerized Gel Glasses for Broadband Vis-NIR Optical Limiting, *ACS Appl. Mater. Interfaces*, 2021, **13**, 897–903.

50 J. G. Croissant, X. Cattoen, J. O. Durand, M. Wong Chi Man and N. M. Khashab, Organosilica hybrid nanomaterials with a high organic content: syntheses and applications of silsesquioxanes, *Nanoscale*, 2016, **8**, 19945–19972.

51 Z. Xie, F. Wang and C. Y. Liu, Organic-inorganic hybrid functional carbon dot gel glasses, *Adv. Mater.*, 2012, **24**, 1716–1721.

52 J. Sun, B. Yuan, X. Hou, C. Yan, X. Sun, Z. Xie, X. Shao and S. Zhou, Broadband optical limiting of a novel twisted tetrathiafulvalene incorporated donor–acceptor material and its Ormosil gel glasses, *J. Mater. Chem. C*, 2018, **6**, 8495–8501.

53 W. Burkhardt, T. Christmann, S. Franke, W. Kriegseis, D. Meister, B. K. Meyer, W. Niessner, D. Schalch and A. Scharmann, Tungsten and fluorine co-doping of VO_2 films, *Thin Solid Films*, 2002, 226–231.

54 Y.-Y. Hu, W.-Q. Li, L. Yang, J.-K. Feng and W. Q. Tian, Electronic properties and nonlinear optical responses of boron/nitrogen-doped zigzag graphene nanoribbons, *Can. J. Chem.*, 2016, **94**, 620–625.

55 I. Papadakis, M. Stavrou, S. Bawari, T. N. Narayanan and S. Couris, Outstanding Broadband (532 nm to 2.2 mum) and Very Efficient Optical Limiting Performance of Some Defect-Engineered Graphenes, *J. Phys. Chem. Lett.*, 2020, **11**, 9515–9520.

56 G. M. Sheldrick, *SHELXS-97, Program for solution of crystal structures*, 1997.
57 G. M. Sheldrick, *SHELXL-97, Program for refinement of crystal structures*, 1997.
58 G. M. Sheldrick, A short history of SHELX, *Acta Crystallogr., Sect. A: Found. Crystallogr.*, 2008, **64**, 112–122.
59 O. W. Howarth, L. Pettersson and I. Andersson, Aqueous Molybdovanadates at High Mo : V Ratio, *J. Chem. Soc., Dalton Trans.*, 1991, 1799–1812.
60 R. I. Maksimovskaya and N. N. Chumachenko, ^{51}V and ^{17}O NMR Studies of the Mixed Metal Polyanions in Aqueous V-Mo Solutions, *Polyhedron*, 1987, **6**, 1813–1821.
61 A. Björnberg, Multicomponent polyanions. 28. The structure of $K_7Mo_8V_5O_{40}.\sim.8H_2O$, a compound containing a structurally new potassium–coordinated octamolybdopentavanadate anion, *Acta Crystallogr., Sect. B: Struct. Crystallogr. Cryst. Chem.*, 1980, **86**, 1530–1536.
62 A. Björnberg, Multicomponent polyanions. 26. The crystal structure of $Na_6Mo_6V_2O_{26}(H_2O)_{16}$, a compound containing sodium–coordinated hexamolybdodivanadate anions, *Acta Crystallogr., Sect. B: Struct. Crystallogr. Cryst. Chem.*, 1979, **35**, 1995–1999.
63 A. Björnberg, Multicomponent polyanions. 22. The molecular and crystal structure of $K_8Mo_4V_8O_{36}.12H_2O$, a compound containing a structurally new heteropolyanion, *Acta Crystallogr., Sect. B: Struct. Crystallogr. Cryst. Chem.*, 1979, **35**, 1989–1995.
64 M. Filowitz, R. K. C. Ho, W. G. Klemperer and W. Shum, ^{17}O Nuclear Magnetic Resonance Spectroscopy of Polyoxometalates. 1. Sensitivity and Resolution, *Inorg. Chem.*, 1979, **18**, 93–103.
65 N. Strukan, M. Cindrid and B. Kamenar, Synthesis and structure of $[(CH_3)_4N]_4[H_2MoV_9O_{28}]Cl{\cdot}6H_2O$, *Polyhedron*, 1997, **16**, 629–634.
66 S. Spillane, R. Sharma, A. Zavras, R. Mulder, C. A. Ohlin, L. Goerigk, R. A. J. O'Hair and C. Ritchie, Non-Aqueous Microwave-Assisted Syntheses of Deca- and HexaMolybdovanadates, *Angew. Chem., Int. Ed.*, 2017, **56**, 8568–8572.
67 I. D. Brown, Recent Developments in the Methods and Applications of the Bond Valence Model, *Chem. Rev.*, 2009, **109**, 6858–6919.
68 N. E. Brese and M. O'keeffe, Bond-Valence Parameters for Solids, *Acta Crystallogr., Sect. B: Struct. Sci.*, 1991, **47**, 192–197.
69 J. Tucher, Y. Wu, L. C. Nye, I. Ivanovic-Burmazovic, M. M. Khusniyarov and C. Streb, Metal substitution in a Lindqvist polyoxometalate leads to improved photocatalytic performance, *Dalton Trans.*, 2012, **41**, 9938–9943.
70 L. Wang, L. Zhu, P. Yin, W. Fu, J. Chen, J. Hao, F. Xiao, C. Lv, J. Zhang, L. Shi, Q. Li and Y. Wei, From 0D dimer to 2D Network-Supramolecular Assembly of Organic Derivatized Polyoxometalates with Remote Hydroxyl via Hydrogen Bonding, *Inorg. Chem.*, 2009, **48**, 9222–9235.
71 C. Rocchiccioli-Deltcheff, M. Fournier, R. Franck and R. Thouvenot, Vibrational investigations of polyoxometalates. 2. Evidence for anion-anion interactions in molybdenum(VI) and tungsten(VI) compounds related to the Keggin structure, *Inorg. Chem.*, 1983, **22**, 207–216.
72 I. R. Lewis and H. G. M. Edwards, *Handbook of Raman Spectroscopy-From the Research Laboratory to the Process Line*, Marcel Dekker, Inc., New York, Basel, 2nd edn, 2001.
73 J. Moulder, W. F. Stickle, P. E. Sobol and K. D. Bomben, *Handbook of X-Ray Photoelectron Spectroscopy*, Perkin Elmer Corporation, Minnesota, 2nd edn, 1992.
74 L. Wang, P. Yin, J. Zhang, J. Hao, C. Lv, F. Xiao and Y. Wei, χ-Octamolybdate $[Mo^{V4}Mo^{VI4}O_{24}]^{4-}$: An Unusual Small Polyoxometalate in Partially Reduced Form from Nonaqueous Solvent Reduction, *Chem. – Eur. J.*, 2011, **17**, 4796–4801.
75 A. B. Ganganboina, A. D. Chowdhury and R. A. Doong, N-Doped Graphene Quantum Dots-Decorated V2O5 Nanosheet for Fluorescence Turn Off-On Detection of Cysteine, *ACS Appl. Mater. Interfaces*, 2018, **10**, 614–624.
76 J. I. Pankove, *Optical processes in semiconductors*, Prentice-Hall, Englewood Cliffs, N.J., 1971.
77 W. M. Wesley and W. G. H. Harry, *Reflectance Spectroscopy*, Wiley, New York, 1966.
78 M. Sheik-bahae, A. A. Said, T.-h. Wei and E. W. V. Stryland, Sensitive Measurement of Optical Nonlinearities Using a Single Beam, *IEEE J. Quantum Electron.*, 1990, **26**, 760–769.
79 G.-K. Lim, Z. L. Chen, J. Clark, R. G. S. Goh, W.-H. Ng, H.-W. Tan, R. H. Friend, P. K. H. Ho and L.-L. Chua, Giant broadband nonlinear optical absorption response in dispersed graphene single sheets, *Nat. Photonics*, 2011, **5**, 554–600.
80 J. Sun, Y. Sun, C. Yan, D. Lin, Z. Xie, Y. Zhou, C. Yuan, H. L. Zhang and X. Shao, Hao-Li Zhang and Xiangfeng Shao Remarkable nonlinear optical response of pyrazine-fused trichalcogenasumanenes and their application for optical power limiting, *J. Mater. Chem. C*, 2018, **6**, 13114–13119.
81 A. A. Said, M. Sheik-Bahae, D. J. Hagan, T. H. Wei, J. Wang, J. Young and E. W. V. Stryland, Determination of bound-electronic and free-carrier nonlinearities in ZnSe, GaAs, CdTe, and ZnTe, *J. Opt. Soc. Am. B*, 1992, **9**, 405–414.

